Chemical Mechanisms Involved in the Coupled Attack of Sulfate and Chloride Ions on Low-Carbon Cementitious Materials: An In-Depth Study

François El Inaty, Mario Marchetti, Marc Quiertant, Othman Omikrine Metalssi

applied sciences

MDPI

Article

Chemical Mechanisms Involved in the Coupled Attack of Sulfate and Chloride Ions on Low-Carbon Cementitious Materials: An In-Depth Study

François El Inaty [1], Mario Marchetti [1], Marc Quiertant [2,*] and Othman Omikrine Metalssi [1]

[1] Unité Mixte de Recherche-Matériaux pour une Construction Durable (UMR MCD), Université Gustave Eiffel, Cerema, F-77454 Marne-la-Vallée, France; francois.el-inaty@univ-eiffel.fr (F.E.I.); mario.marchetti@univ-eiffel.fr (M.M.); othman.omikrine-metalssi@univ-eiffel.fr (O.O.M.)
[2] Laboratoire Expérimentation et Modélisation pour le Génie Civil et Urbain (EMGCU), Université Gustave Eiffel, F-77454 Marne-la-Vallée, France
* Correspondence: marc.quiertant@univ-eiffel.fr

Abstract: This study aims to analyze the individual and combined chemical attacks of sulfate and chloride ions on cementitious materials and assess the efficiency of some selected additives (fly ash, blast furnace slag, and metakaolin) in countering this combined attack. This research is conducted in the context of construction in marine environments, where reinforced concrete structures are often subject to significant challenges due to early exposure to sulfate and chloride ions. This early exposure results in concrete expansion, cracking, and, ultimately, the corrosion of steel reinforcements. Nevertheless, the interaction between sulfate ions, chloride ions, and the cementitious matrix remains poorly understood. Previous research has drawn conflicting conclusions, with some suggesting that sulfate ions mitigate chloride attacks, while others have come to the opposite conclusion. During this study, experimental investigations were conducted by immersing powders obtained from crushed ordinary Portland cement (CEM I) paste specimens, as well as binary, ternary, and quaternary blends, in sulfate, chloride, and sulfate–chloride solutions over the course of 25 days at an early age. Results from different characterization techniques (thermogravimetric analysis, Fourier Transform Infrared spectroscopy, Raman spectroscopy, etc.) indicate that chloride ions delay the formation of ettringite, while the presence of sulfate ions accelerates the chloride attack by limiting the formation of Friedel's salt. The Mercury Intrusion Porosimetry test confirmed these results by showing a pronounced increase in specimens' porosity after exposure to solely sulfate after 25 days, compared to the ones exposed to both sulfate and chloride ions. Furthermore, the incorporation of multiple additives, particularly in ternary and quaternary blends, demonstrates the enhanced durability of the studied samples. This was confirmed by a Fourier Transform Infrared spectroscopy analysis, which indicated a delayed ettringite formation in these mixtures. This delay was further affirmed by the complete depletion of sulfate ions in the sulfate solutions upon contact with powders derived from the 100% CEM I paste.

Keywords: durability; sulfate; chloride; supplementary cementitious materials; early age; coupling

Citation: El Inaty, F.; Marchetti, M.; Quiertant, M.; Omikrine Metalssi, O. Chemical Mechanisms Involved in the Coupled Attack of Sulfate and Chloride Ions on Low-Carbon Cementitious Materials: An In-Depth Study. *Appl. Sci.* **2023**, *13*, 11729. https://doi.org/10.3390/app132111729

Received: 28 September 2023
Revised: 23 October 2023
Accepted: 24 October 2023
Published: 26 October 2023

1. Introduction

In recent decades, researchers have been increasingly interested in the durability of Reinforced Concrete (RC) structures [1,2]. Essentially, this refers to the ability of such structures to maintain their original form, serviceability, and quality over time [3]. During their operational lifespan, RC structures not only encounter mechanical loads but also endure physical and chemical deterioration caused by environmental factors such as carbonation, sulfuric acid, sulfate and/or chloride-enriched environments, freeze–thaw cycles, etc., that alter their durability [1,4,5]. Numerous researchers have observed that changes in the durability of RC structures result from the combined influence of various

factors, whether they be mechanical loadings or environmental factors. As a result, they have devoted their research efforts to investigating the combination of these factors [6–9]. Marine environments expose RC structures to both sulfate and chloride ions. This has been identified as a significant challenge by several researchers [9–11].

1.1. Literature Review and Research Significance

Sulfate ions penetrate the cementitious matrix and react with hydrated products. These reactions lead to the formation of ettringite and/or gypsum. These products are primarily responsible for concrete expansion and cracking. The formation of these chemical compounds induces internal pressure within the concrete matrix, leading to structural deterioration and compromising its long-term integrity [12–14]. Nevertheless, unbound chloride ions within the cement matrix, such as Friedel's salt, remain free and contribute to the corrosion of steel reinforcing bars (rebars). This corrosion not only weakens the structural integrity of the steel rebars, but also generates corrosion products that occupy a larger volume than the original steel, thereby leading to the gradual expansion and cracking of the surrounding concrete over time [15,16]. The cumulative effects of such processes raise challenges to the durability and performance of RC structures. Presently, the individual attack mechanisms of sulfate and chloride ions are well understood [17–21]. However, when these ions are combined, the degradation processes and the causes of deterioration undergo significant changes due to the interaction between sulfate and chloride ions [9].

According to a study conducted by Stroh et al. [22], the penetration of chloride ions into the cement matrix occurs prior to that of sulfate ions. Friedel's salt is formed first during this sequence. Subsequently, sulfate ions migrate into the cement matrix and undergo a reaction with the hydrated cement products, resulting in the formation of gypsum. This process reduces the pH within the material, which, in turn, triggers the degradation of the previously formed Friedel's salt. Furthermore, the excess of sulfate ions contributes to the creation of ettringite. This sequence of events demonstrates the complex interaction between chloride and sulfate ions in the concrete environment. Indeed, a study conducted by Stroh et al. revealed an interesting observation regarding the interaction between sulfate and chloride ions. According to their findings, sulfate in the concrete matrix reduces chloride ions' binding capacity. As a consequence of this reduced binding, the attack by chloride ions is accelerated, which leads to an even more rapid and severe corrosion of the steel rebars within RC structures.

On the one hand, some studies [23–26] support the idea that sulfate leads to the destabilization of Friedel's salt and reduces the binding capacity of chloride. As a result, the chloride ions' attack is accelerated. On the other hand, some other studies [27,28] contradict this claim. They propose that sulfate ions actually attenuate chloride diffusion in concrete by decreasing its porosity.

Regarding the impact of chloride on sulfate, some studies have observed that the presence of chloride ions inhibits the effect of external sulfate attack (ESA) on concrete. In contrast, the effect of chloride ions on ettringite formation is an area where research is still lacking, as noted by Ran et al. [29]. The combined attack is influenced by several factors, including the porosity of the specimens, the types and concentrations of chloride and sulfate ions, including the cation type, the chemistry of the binder (characteristics of the pozzolan and its level of replacement), the duration of exposure, etc. [11,25,30,31].

Furthermore, construction materials have been criticized for their substantial contribution to high carbon dioxide (CO_2) emissions and natural resource depletion [32]. By the year 2010, cement alone was responsible for approximately 36% of the total 7.7 billion metric tons of CO_2 emissions originating from the construction industry [33]. Consequently, concrete, which heavily relies on cement as a primary component, has emerged as the second-largest contributor to global CO_2 emissions [34]. The significant environmental impact of concrete has led to a growing awareness of the urgent need for sustainable, cost-effective, and eco-friendly alternatives in the construction sector, which Supplementary Cementitious Materials (SCM) have been identified as. This could have an effect on the

durability of RC structures, including with regard to the coupling effect of sulfate and chloride, as previously mentioned.

1.2. Objectives and Scope of the Work

This study seeks to gain deeper insights into the chemical interactions between chloride ions and sulfate ions during coupled attacks on cementitious materials, as well as their reciprocal effects. Additionally, it aims to assess the durability of low-carbon cementitious materials in the context of these interactions. To achieve these objectives, samples of pure cement, as well as binary, ternary, and quaternary blended pastes, were exposed to chloride, sulfate, and chloride–sulfate solutions for 25 days. The investigation employed various characterization methods, including Raman spectroscopy to analyze the solutions, thermogravimetric analysis (TGA), Fourier Transform Infrared spectroscopy (FTIR), and Mercury Intrusion Porosimetry (MIP). Furthermore, the pH levels of the solutions were continuously monitored throughout the experiment.

2. Materials and Methods

2.1. Materials

The cement selected for this research was a CEM I 52.5 N CE CP2 NF produced by EQIOM. Its chemical composition, given by the manufacturer, is shown in Table 1. The proportions of different clinker phases (C_3S = 56.5%, C_2S = 15.8%, C_3A = 5.0%, and C_4AF = 11.6%) were determined using the Bogue formula [35]. Additionally, fly ash and blast furnace slag were also incorporated, and their chemical compositions are detailed in Table 1. Furthermore, metakaolin of the BASF MetaMax type was used in this study. According to the manufacturer, it consisted of 100% calcined kaolin.

Table 1. Chemical compositions of the used CEM I and supplementary cementitious materials as given by the manufacturer.

Components	CEM I (Wt%) [1]	Fly Ash (Wt%) [1]	Blast Furnace Slag (Wt%) [1]
SiO_2	20.38	70.83	35.71
Al_2O_3	4.30	24.36	10.65
Fe_2O_3	3.80	2.24	0.45
TiO_2	0.24	1.48	0.73
MnO	0.08	0.05	0.23
CaO	62.79	0.06	43.32
MgO	1.25	0.23	3.97
SO_3	3.46	-	3.06
K_2O	0.73	0.64	0.45
Na_2O	0.35	0.1	0.16
P_2O_5	-	0.05	0.02
S^{2-}	Traces	-	-
Cl^-	0.05	-	-
Loss of ignition	2.54	-	-
Free lime	1.39	-	-

[1] Weight percent.

When compared to the other additives, CEM I cement has the highest CaO content and the lowest Al_2O_3 and SiO_2 contents. On the other hand, blast furnace slag exhibits a higher CaO content than fly ash.

2.2. Design of Cementitious Material Blends

In this study, various cement pastes were prepared using Portland cement only, as well as binary, ternary, and quaternary blends, with varying ratios of SCM, as shown in Table 2. The selection of these formulations was based on chemical criteria while considering the standardized types of cement specified in NF EN 197-1 [36], which include CEM I to CEM VI types. In all of the mixes, a water-to-binder (w/b) ratio of 0.55 was employed. This

high w/b ratio was used to accelerate the chemical attacks on the material without causing any segregation issues.

Table 2. Composition of the mixes.

	CEMI	Blast Furnace Slag	Metakaolin	Fly Ash
Mix1 (Reference)	100%	-	-	-
Mix2	55%	45%	-	-
Mix3	55%	35%	10%	-
Mix4	55%	20%	10%	15%

2.3. Sampling and Exposure

Prismatic paste specimens measuring 40 × 40 × 160 mm^3 were prepared from each of the four mixtures. The mixing was inspired by the guidelines of the French standard NF EN 196-1 [37]. Binders and water were initially blended at a low rotational speed of 100 revolutions per minute (rpm) for a duration of 60 s. Subsequently, the mixing device was switched to a high-speed setting of 300 rpm for 30 s. Following this, the mixer was deactivated, and a scraping process was executed for 90 s. The entire mixture was then re-mixed at the high-speed setting for an additional 60 s. The resulting paste was uniformly poured into molds in a single layer. It is worth noting that the only method of inducing vibrations during this process involved the application of four external shocks on the mold using a hammer. After a curing period of 24 h, the samples were removed from their molds and manually ground at room temperature (~22 °C) until the particle sizes were reduced to less than 2.5 mm, as shown in Figure 1a. This step aimed to increase the surface area for an increased interaction between the cementitious materials and the sulfate and chloride ions present in the aqueous solutions.

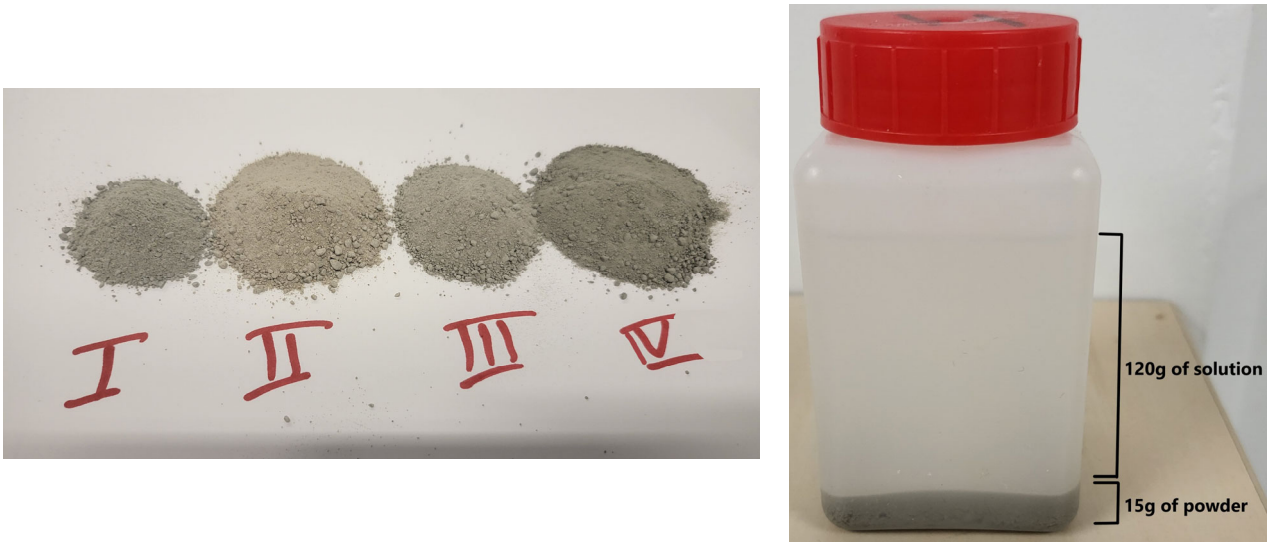

(**a**) (**b**)

Figure 1. (**a**) The powders obtained from the 4 mixes after grinding the specimens and (**b**) the exposure immersion set up.

Subsequently, 15 g of powder from each specimen was completely immersed in 120 g of tap water (EXP0), sodium chloride solution (30 g/L) (EXP1), sodium sulfate solution (15 g/L) (EXP2), and sodium sulfate (15 g/L)–sodium chloride (30 g/L) solution (EXP3), yielding a solution to solid ratio of 8 (Figure 1b). This immersion allowed for the exposure of cementitious materials to the respective solutions. This facilitated the investigation of the chemical effects of chloride and sulfate ions on the specimens. EXP0 served as the reference exposure, EXP1 was used to assess the effect of chloride alone, EXP2 was employed to

evaluate the individual effect of sulfate, and EXP3 was utilized to examine the combined effects of chloride and sulfate, representing the central focus of this study.

2.4. Experimental Methods

2.4.1. Chemical Characterizations

Three methods of chemical characterization were employed to reach a comprehensive understanding of the chemical processes involved in the combined sulfate–chloride attack. Thermogravimetric analysis (TGA) was primarily performed to quantify the presence of portlandite by observing sample mass variations with respect to temperature variation. The measurements were conducted using a NETZSCH STA449 F1 instrument in an inert nitrogen environment, with a temperature range from 25 to 1250 °C and a heating rate of 10 °C per minute. The derivative of the thermogravimetric analysis curve (DTG) was obtained to identify significant mass variations, such as losses or gains.

Fourier Transform Infrared spectroscopy (FTIR) was also employed to characterize the chemical composition of the cementitious materials, qualitatively identifying chemical bonds present in the materials. Measurements were obtained using a Nicolet iS50 spectrometer, covering a spectral range of 400 to 4000 cm^{-1}. The obtained bands were compared to those found in the literature.

Furthermore, Raman spectroscopy was utilized to evaluate the depletion of sulfate ions in the solutions. The Raman spectrometer used was an iRaman by BWTek, equipped with a 50 mW output 532 nm laser. The instrument operated in the spectral range of 150–4000 cm^{-1}, with a spectral resolution of 4 cm^{-1}. It was equipped with an immersion probe for analyzing the solutions and monitoring the consumption of sulfate ions during various stages of the chemical attack. The integration time was set at 15 s, and each obtained spectrum was the average of two spectra.

These three methods were applied to both the powder samples (TGA and FTIR) and the solutions (Raman spectroscopy) after respective exposure durations of 1 (T1), 2 (T2), 5 (T3), 11 (T4), 18 (T5), and 25 days (T6). The combined use of these three methods led to a better understanding of the chemical composition of the samples. This was crucial for analyzing the chemical effects resulting from the coupled interaction of chloride and sulfate ions with a cementitious matrix.

Additionally, the pH of the solutions was measured using a Mettler Toledo pH meter at room temperature (~22 °C) at the same time intervals as those chosen for the other analysis methods. The pH results were double-checked using Universal Indicator pH-indicator papers. The studies conducted by Mehta et al. [38] and Brown et al. [39] have highlighted the significant impact of sulfate attacks on the pH of surrounding solutions and vice versa. During sulfate attacks on cementitious materials, sulfate ions react with calcium hydroxide ($Ca(OH)_2$), calcium aluminate, and low-sulfate calcium sulfo-aluminate, leading to the formation of expansive compounds. This, in turn, can cause expansion and cracking in RC structures. A key finding from these studies is that the chemical reaction between sulfate and concrete generates hydroxyl ions, which subsequently increase the pH of the surrounding solution. The concentration of sulfate in the solution was observed to correlate with the liberation of hydroxyl ions. This relationship is linked to sulfates replacing the two moles of hydroxyl during their interaction with concrete, leading to an increase in pH. The interplay between sulfate attacks and pH variations is a critical aspect of understanding the degradation mechanisms in cementitious materials.

Indeed, the study conducted by Delagrave et al. [40] has interpreted the influence of chloride attacks on the leaching of calcium into surrounding solutions. The presence of chloride ions can promote the release of calcium from cementitious materials, leading to its dissolution into the surrounding solution. For this, the pH of the solution was measured using a pH meter after 1, 2, 5, 11, 18, and 25 days of exposure.

2.4.2. Microstructural Characterizations

To gain a deeper understanding of the chemical changes resulting from the combination of sulfate and chloride on cementitious materials, a microstructural porosity analysis was conducted using an MIP test on the attacked powder after 1 and 25 days of exposure. This test not only provided information about the total porosity but also offered insights into the size distribution of pores within the material. This allowed us to gain valuable data on the pores' characteristics and distribution.

The MIP test was performed using the Micrometrics Autopore IV 9520 Porosimeter instrument. The procedure began by evacuating all of the air present in the penetrometer, followed by filling it with mercury at a low pressure (0.1 MPa). Subsequently, the pressure was increased to facilitate mercury penetration into the material's pores. Finally, the penetrometer was immersed in hydraulic fluid under high pressure (reaching 414 MPa).

Before conducting the MIP test, a specific pre-treatment procedure was applied to the specimens. Initially, the samples were submerged in liquid nitrogen for 10 min. This step aimed to ensure thermal equilibrium, indicating that the water within the pores had solidified completely. Subsequently, the specimens were placed under vacuum conditions at −46 °C for 72 h. This lyophilization process pre-treated the samples by drying them, effectively arresting the cement hydration.

3. Results

3.1. pH Variations

The results of pH variation as a function of time are shown in Figure 2.

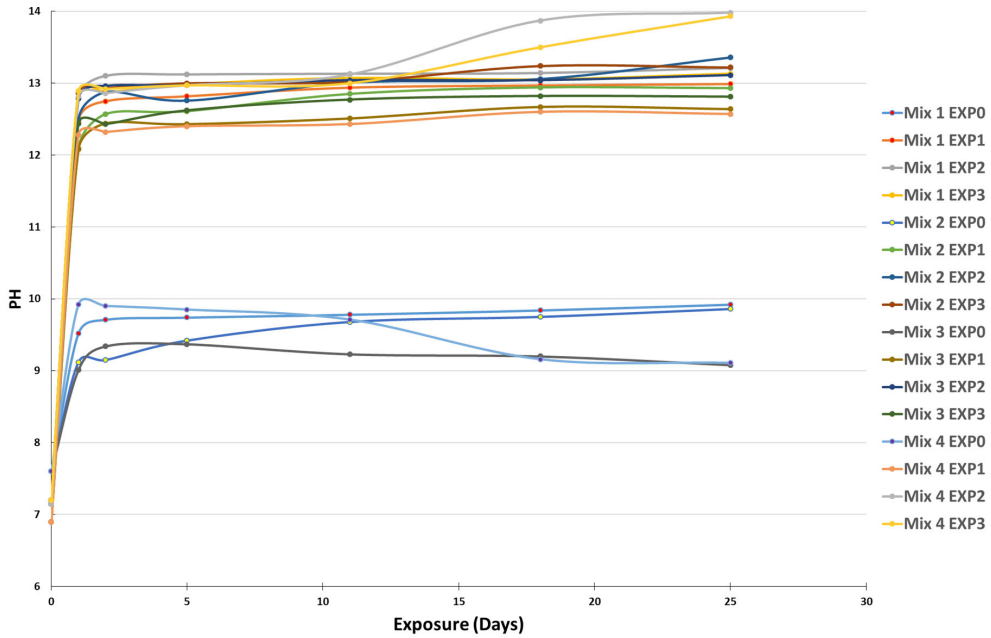

Figure 2. pH variation of the four different mixes after being exposed to the four different environments at different exposure times.

The curves demonstrate a significant increase in the pH of the solutions after submerging the cement paste powders in the four different environments. In the case of EXP0 (tap water only), the pH rose from 7.6 to a range of 8–9 after 1 day of contact between the water and the specimens, stabilizing with negligible fluctuations over the subsequent 24 days of exposure. This increase was due to the alkalinity of the submerged pastes [41]. For the other exposures (EXP1, EXP2, and EXP3), the pH increase was even more pronounced, ranging from 6.9–7.2 to 12.5–14, and was directly related to the leaching of calcium and hydroxyl ions into the solutions [38–40], as previously mentioned in Section 2.4.1. The chemical reaction between sulfate and cementitious materials resulted in the generation of hydroxyl

ions, which subsequently elevated the pH of the surrounding solution. Sulfates replace two moles of hydroxyl during their interaction with concrete, thereby causing an increase in the pH. Additionally, chloride ions affect pH levels. The presence of chloride ions can facilitate the release of calcium from cementitious materials, leading to its dissolution into the adjacent solution. This phenomenon further contributes to pH changes. Understanding the interplay between sulfate and chloride ions and their impacts on pH variations is crucial for a comprehensive grasp of the intricate deterioration processes occurring within cementitious materials.

In the case of EXP1 (chloride-only exposure), the pH was the lowest compared to EXP2 and EXP3, because chloride does not influence pH in the way sulfate does, due to the kinetics of the chemical reactions. On the other hand, EXP2 (sulfate-only exposure) exhibited the highest pH among the different exposures. The decomposition of calcium hydroxide and calcium–silicate–hydrate compounds can significantly elevate the pH of the surrounding solution [42,43]. This observation suggests that hydroxyl and calcium leaching is the most significant when cementitious materials are exposed to sulfate alone, and the coupling of chloride and sulfate attenuates the attack since the pH of EXP3 always ranged between the values of the pH of EXP1 and EXP2, even though both chloride and sulfate increase pH levels. Notably, the differences in pH between the various mixes were not considerable.

When comparing the various mixtures, it was evident that the incorporation of SCM caused a comparatively lower increase in pH compared to Mix1, composed entirely of CEM I. SCM plays a role in reducing the presence of calcium hydroxide, often referred to as portlandite [44]. This reduction results in the decreased leaching of calcium and hydroxyl ions into the solution, consequently leading to a less pronounced rise in the pH of the surrounding environment.

Overall, these pH variations provide valuable insights into the chemical reactions and leaching processes occurring in cementitious materials when exposed to different environments.

Furthermore, it is worth noting that in the presence of sulfate (EXP2 and EXP3), a change in color and the formation of a thin white film were observed on the surface of the submerged powders after 11 days of exposure (as shown in Figure 3). These visible changes indicate the occurrence of chemical reactions within the cementitious materials. The formation of a white film is likely associated with the precipitation of compounds resulting from the reaction between sulfate ions and the cementitious matrix. According to other studies, it is more common for gypsum to build up on the surface of the material [45,46]. All of the present solids have been filtered and analyzed together.

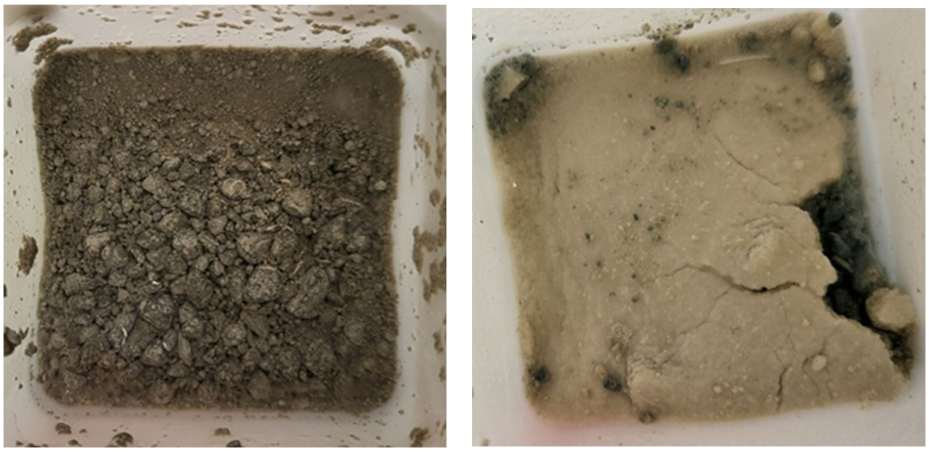

(**a**) (**b**)

Figure 3. Tested powders originating from Mix1 after 11 days of exposure to (**a**) water (EXP0) and (**b**) sulfate (EXP2).

3.2. Thermogravimetric Analysis

A TGA was conducted on the four mixes after 1, 2, 5, 11, 18, and 25 days of exposure following their removal from the solutions and subsequent drying at 55 ± 5 °C for 24 h (see Figure 4). In accordance with previous research findings [47,48], it was assumed that the first peak or major mass loss observed between 30 °C and 200 °C is related to the decomposition of ettringite, calcium silicate hydrate (C-S-H), and free water elimination. Additionally, the presence of monosulfoaluminates (AFms) is indicated by a peak at 190 °C. A third peak, occurring between 450 °C and 550 °C, corresponds to the dihydroxylation process of portlandite or calcium hydroxide ($Ca(OH)_2$), while a peak between 650 °C and 820 °C is attributed to the decarbonization of calcite ($CaCO_3$). The thermogravimetric derivative (DTG) was obtained to quickly identify the peaks.

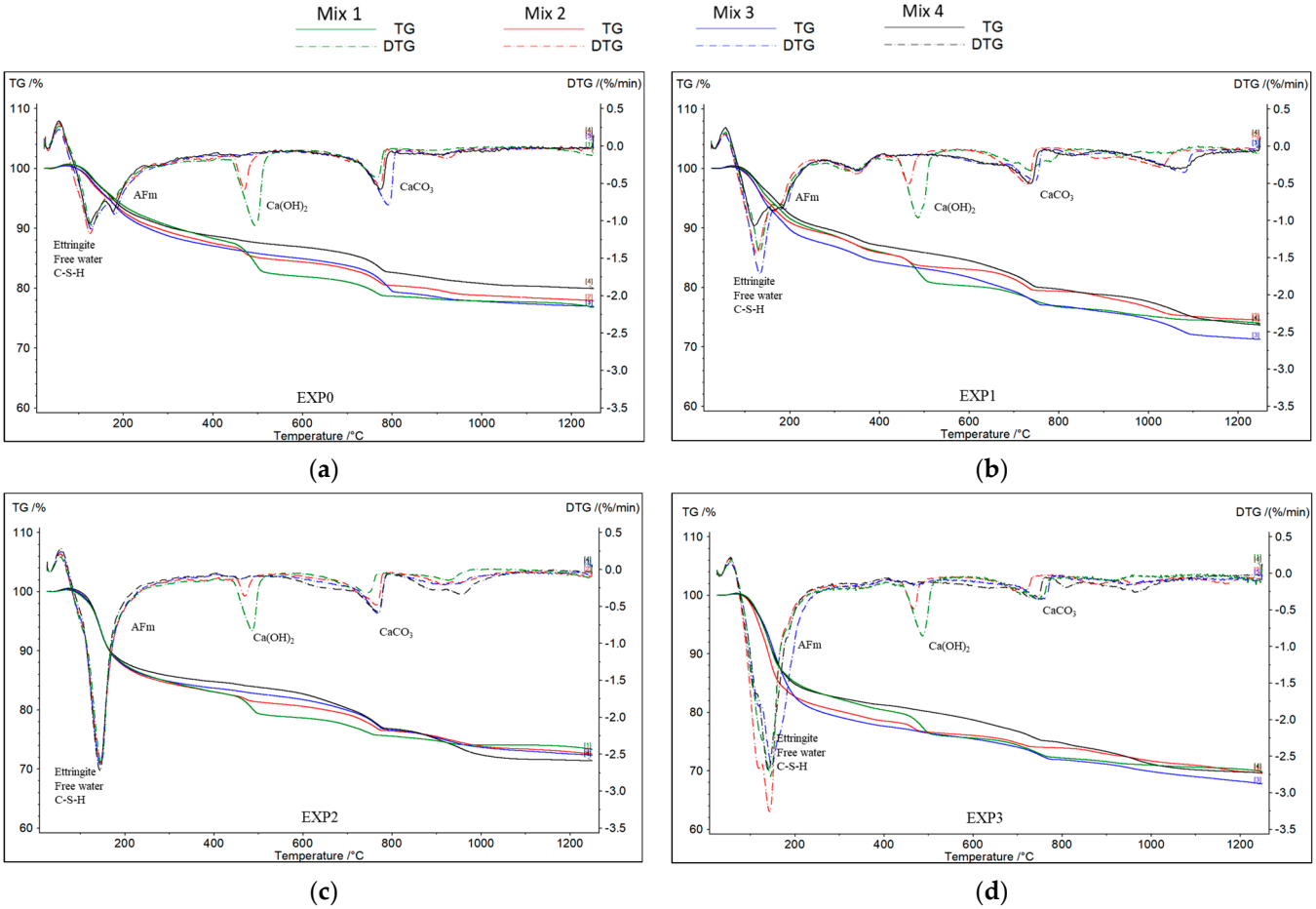

Figure 4. TGA and DTG of the four mixes after 25 days of exposure to (**a**) water, (**b**) chloride, (**c**) sulfate, and (**d**) sulfate–chloride.

In this study, portlandite losses were quantified and are presented in Table 3. Moreover, careful observation was made regarding the AFm peaks (as represented in Figure 4). This approach is crucial because, in addition to the reasons discussed in Section 3.1, portlandite and AFm, in the presence of sulfate ions, are known to participate in the formation of expansive products [49,50].

Table 3. Portlandite consumption (%) in the four mixes over time and in different exposure conditions.

Mixes	EXP	Day 1	Day 2	Day 5	Day 11	Day 18	Day 25	D25–D1
Mix1	0	3.92	5.08	5.19	4.82	5.54	5.68	1.76
Mix1	1	3.90	4.69	3.82	3.96	4.40	4.89	0.99
Mix1	2	3.53	3.93	3.70	3.20	2.85	3.32	−0.21
Mix1	3	3.50	3.79	3.35	3.62	3.04	3.44	−0.06
Mix2	0	2.28	2.05	1.78	1.91	1.75	1.96	−0.32
Mix2	1	2.01	1.79	1.72	1.64	1.56	1.87	−0.14
Mix2	2	1.67	1.43	1.1	1.06	1.09	0.91	−0.76
Mix2	3	1.60	1.41	1.12	1.12	1.21	1.02	−0.58
Mix3	0, 1, 2, and 3	Negligible						NA [1]
Mix4	0, 1, 2, and 3	Negligible						NA [1]

[1] Not available.

As shown in Table 3, Mix2 experienced a loss of portlandite when immersed in water, chloride, sulfate, or a combination of chloride and sulfate solutions. On the other hand, Mix1 experienced the loss of portlandite only when in contact with sulfate and the combination of sulfate and chloride. This loss can be attributed to the consumption of portlandite by chloride and sulfate ions, particularly evident in EXP1, EXP2, and EXP3. The loss of portlandite in Mix2 at EXP0, and its absence in Mix3 and Mix4 in all four exposure conditions, even though the pastes were at an early age (the hydration process of cementitious materials was still ongoing), might contribute to the pozzolanic effect of SCM, which leads to calcium hydroxide consumption [51].

While comparing the loss of portlandite content under different exposure conditions, it was noted that the highest loss occurred when the mixes (Mix1 and Mix2 in this case) were exposed solely to sulfate (EXP2). This finding indicates that the coupling of the two ions (chloride and sulfate) in EXP3 mitigated the attack and resulted in a lesser reduction in portlandite content.

As shown in Figure 4, the disappearance of AFm in the pastes subjected to only sulfate ions suggests that the sulfate attack led to the consumption or transformation of AFm compounds. AFm is recognized as relatively less stable and is generated through the hydration of C_3A and C_4AF [52]. Subsequently, when the aluminate reacts with gypsum, the formation of AFt occurs [53]. However, interestingly, when both chloride and sulfate ions were present together (EXP3), AFm was still present after 25 days of exposure when compared to exposure to sulfate ions alone (EXP2). This indicates that the coupling of chloride and sulfate ions in the solution has a protective effect and mitigates the deterioration of cementitious materials.

It is important to note that while an increase was observed in the mass loss associated with the first DTG peak (at T < 200 °C), as illustrated in Figure 4, which represents the quantities of free water, C-S-H, and ettringite in the presence of sulfate (EXP2 and EXP3), the results were not consistently conclusive. This ambiguity arises from the simultaneous presence of free water, the decomposition of C-S-H, and the formation of ettringite. The observed increase in mass loss at T < 200 °C in EXP2 and EXP3 (where sulfate was present) substantiates that, in addition to the decalcification of C-S-H, a significant amount of ettringite did indeed form.

3.3. Raman Spectroscopy

Raman spectroscopy was employed to assess the consumption and/or depletion of sulfate ions in the EXP2 and EXP3 solutions. The vibrational mode of SO_4^{2-} ions was identified around the spectral region of 1000 cm^{-1} [54]. Moreover, the vibration of water molecules was identified at around 3400 cm^{-1}, due to the vibration of O-H band, as shown

in Figure 5 [55]. The results demonstrate that the sulfate ions present in the solutions were not fully consumed, even after a 25-day exposure, except for in the EXP2 solution containing Mix1 (100% CEMI). In this case, the sulfate ions were completely consumed within just 11 days (Figure 5). When simultaneously exposed to both sulfate and chloride ions, the peak at 1000 cm^{-1} was still present. This suggests that the presence of chloride ions mitigates the effect of sulfate ions, and that mixtures containing SCM exhibit an improved resistance to the studied attacks.

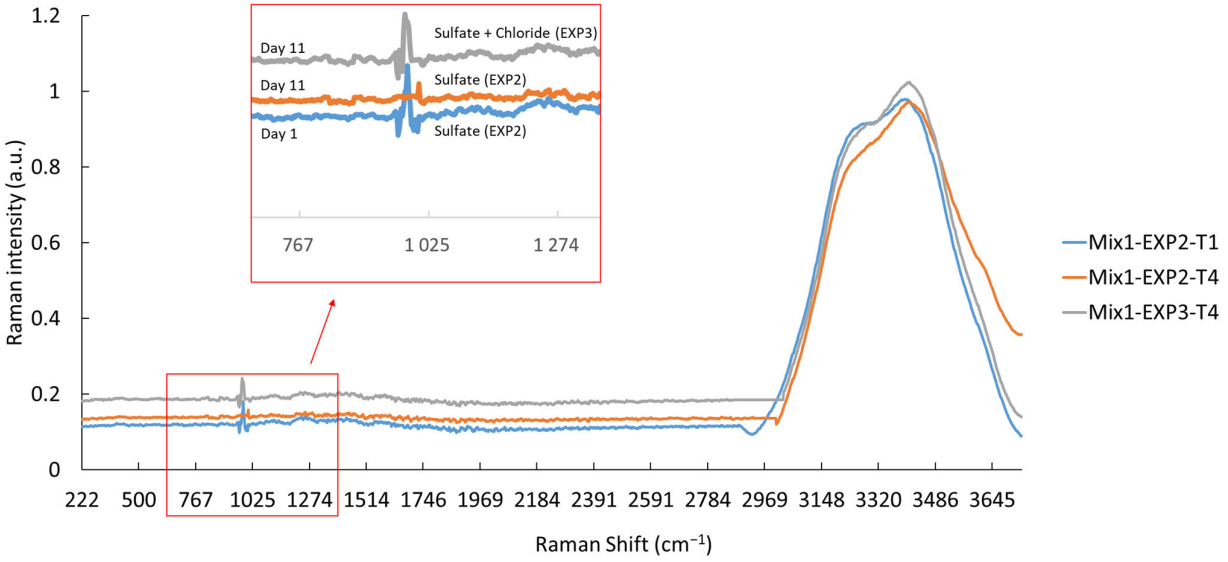

Figure 5. Raman spectra of Mix1 (100% CEMI) after 1 and 11 days of exposure to sulfate (EXP1) and sulfate–chloride (EXP3).

3.4. Fourier Transform Infrared Spectroscopy

According to previous studies [56–58], specific absorption bands can be associated with certain compounds. Portlandite, or $Ca(OH)_2$, is typically found around 3642 cm^{-1}, attributed to O-H stretching. The S-O bond (sulfate phases) stretch from gypsum, ettringite, and monosulfoaluminates is indicated at 1102 cm^{-1}. Ettringite, in particular, produces a band at 610 cm^{-1} corresponding to the S-O stretch. Water can be detected by the broad band at 3373 cm^{-1}. Gypsum generates a band at 1680 cm^{-1}, attributed to O-H stretching. The presence of calcite and Friedel's salt can be identified by the band at 1440 cm^{-1}, which indicates C-O stretch. The SiO_4 stretch, observed around 967 cm^{-1}, corresponds to C-S-H, calcium aluminate hydrates, and H_2O. Additionally, Friedel's salt can be identified around 810 cm^{-1}, which refers to the stretching vibration of the Al-O bond in the material. Our FTIR test results are shown in Figure 6.

The analysis of FTIR spectra provided valuable insights into the chemical reactions occurring in the different mixes under various exposure conditions. As illustrated in Figure 6, the peak at 3642 cm^{-1}, indicative of portlandite, showed that its presence diminished over time due to exposure to chloride ions. In Mix2, portlandite disappeared after 25 days, while in Mix3 and Mix4, it vanished after 11 days and 5 days of exposure, respectively. Although the TGA did not detect this compound in Mix 3 and Mix 4, FTIR analysis revealed its presence in those mixes. This might be due to its presence in low quantities. In the case of chloride exposure (EXP1), the presence of Friedel's salt was detected from the first day, explaining the consumption of portlandite in this exposure condition. Notably, the peak at 810 cm^{-1}, representing Friedel's salt, was absent when sulfate was present along with chloride (EXP3) (refer to Figure 7). This observation aligns with previous studies [11,25] that have demonstrated the instability of Friedel's salt in the presence of sulfate. This phenomenon was attributed to the substitution of chloride ions (Cl^-) by sulfate ions (SO_4^{2-}), leading to its transformation into AFt. However, it is worth noting that the chloride ions

bonded to C-S-H were not destabilized by Na_2SO_4, as the quantity of this bound chloride was minimal. Furthermore, it is also worth noting that the pH drop in the concrete itself (not the surrounding solution), resulting from a sulfate attack, contributed to the destabilization of Friedel's salt [22].

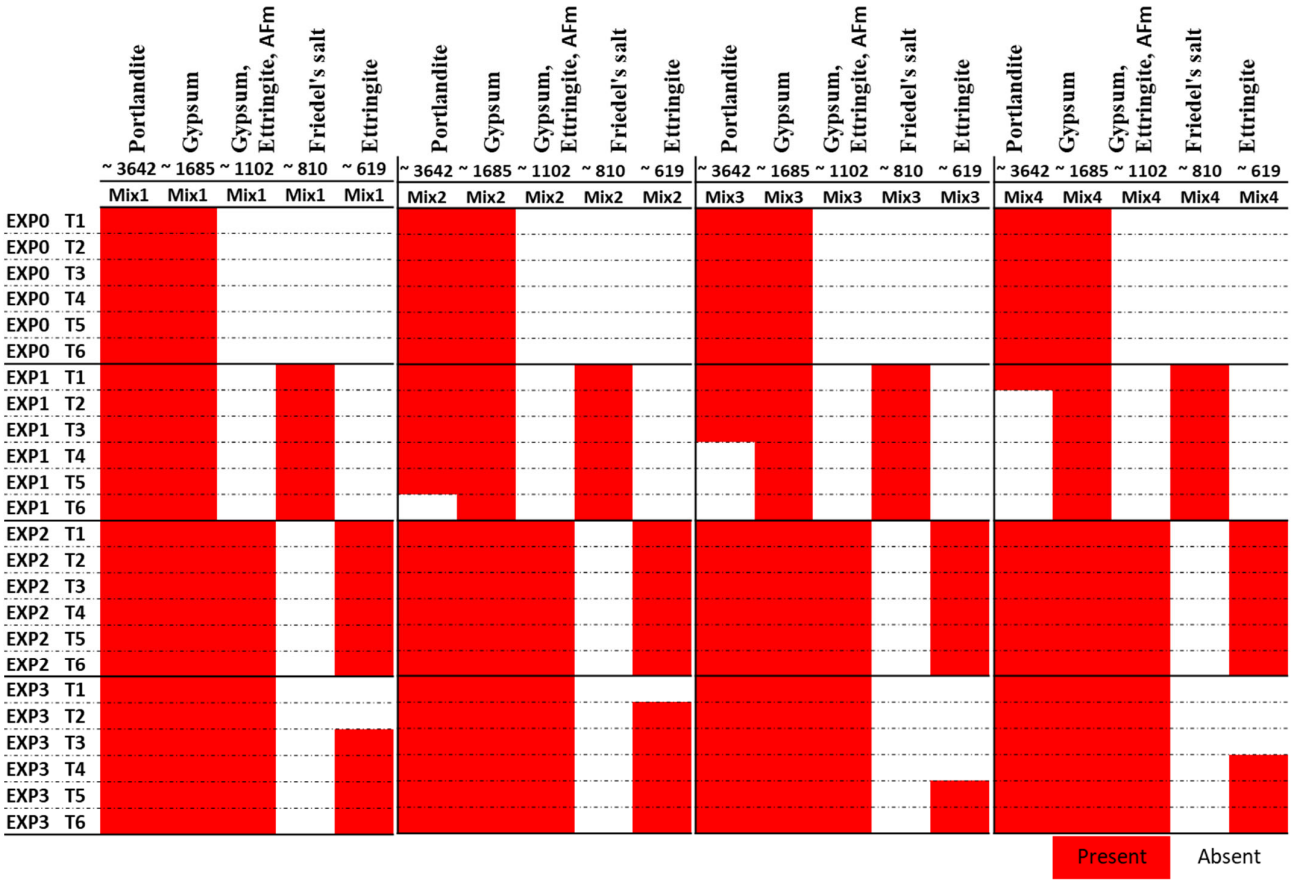

Figure 6. Functional groups (identified by FTIR in cm^{-1}) present in the four mixes after different exposure duration to the considered exposure environments.

The peak at 1685 cm^{-1}, corresponding to gypsum, was consistently present in all of the mixes due to the presence of gypsum in the pastes. The peak at 1102 cm^{-1} was observed in all mixes when sulfate was present (as shown in Figure 7). This indicates the formation of gypsum and ettringite, resulting from the chemical reaction between the hydrated products and sulfate ions.

The peak at 619 cm^{-1}, attributed to ettringite, was present in all mixes when only exposed to sulfate. However, its formation was delayed in the presence of both sulfate and chloride. It appeared after 3 days in Mix1, 1 day in Mix2, 18 days in the Mix3, and 11 days in the Mix4.

These results suggest that the presence of sulfate destabilized Friedel's salt and that the presence of chloride, along with sulfate, retarded the formation of ettringite. This implies that chloride attenuates the effect of sulfate attack while reducing the binding capacity of chloride.

Comparing the four mixes in terms of chemical reactions was challenging, as they were attacked at an early age before completing the hydration process. However, the incorporation of more than one SCM (Mix3 and Mix4) appeared to delay the formation of ettringite, indicating the potential benefits of utilizing multiple SCMs to improve the durability of cementitious materials under aggressive exposures.

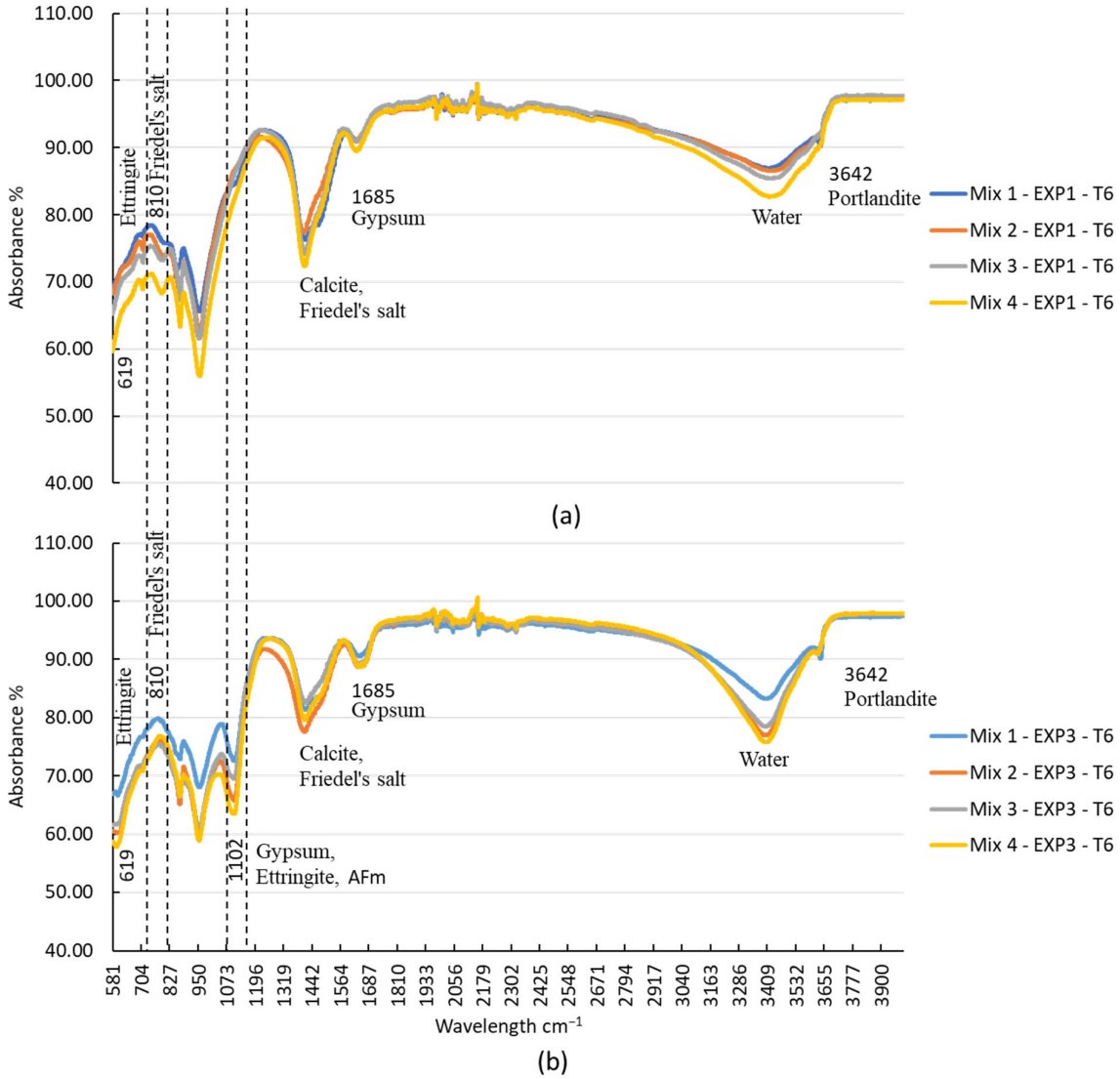

Figure 7. FTIR spectra of the four mixtures after 25 days of exposure to (**a**) chloride and (**b**) sulfate–chloride.

3.5. Mercury Intrusion Porosimetry

MIP measurements were performed on the powders 1 day and 25 days after being submerged in each of the four different exposure environments. The results of these measurements are shown in Figures 8 and 9. This analysis aimed to validate the chemical changes occurring within the samples' microstructures. The characterization focused on assessing total porosity as well as its distribution. According to the existing literature [3,59], the pores within cement paste samples can be categorized into distinct zones:

- Micropores or gel pores, spanning from 1 nm to around 10 nm, emerge as a result of the hydration process. These pores are influenced by factors such as the interlayer spacing of calcium hydroxide and calcium–silicate–hydrate, the type of binders employed, curing conditions, water-to-binder ratio, and the age of the specimens.
- Pores ranging from 10 nm to 100 nm are referred to as small to medium capillary pores. These pores originate from water-filled spaces and are notably impacted by the w/b ratio and the degree of hydration.
- Large capillary pores, spanning between 100 nm and 10 µm, are water-filled and also filled due to C-S-H particle aggregation.
- Macropores have a diameter exceeding 10 µm in size and typically contain entrapped air within the paste. The characteristics of these pores are influenced by the presence of additives, the w/b ratio, the workability of the mixture, and the fabrication process.

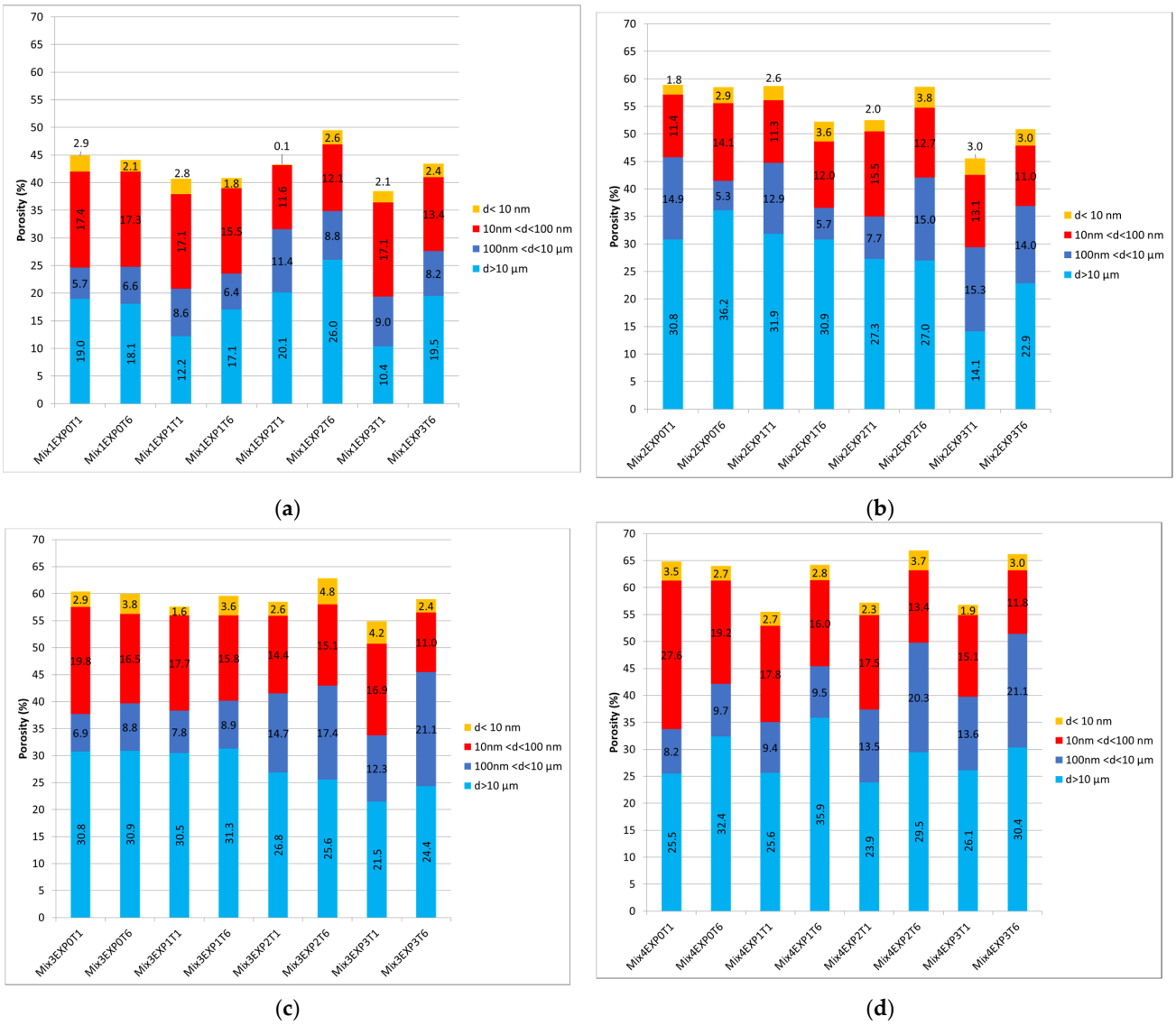

(**a**) (**b**)

(**c**) (**d**)

Figure 8. The total porosity and its distribution at both day 1 and day 25 under different exposure conditions for (**a**) Mix1, (**b**) Mix2, (**c**) Mix3, and (**d**) Mix4.

Upon analyzing the total porosity of the extracted powders after exposure, a distinct pattern emerged. Mix1, consisting solely of CEMI, exhibited the lowest porosity level in this context, ranging from 40% to 45%. In contrast, the porosity levels of the other mixes fell within the range of 55% to 65%. To gain deeper insights into the factors contributing to this rise in porosity when substituting cement with alternative binders, it is imperative to delve into the distribution of porosity across different size ranges. Examining the porosity distribution, it becomes evident that the increase primarily occurred in the macropores, attributed to entrapped air. The formation of these pores was significantly influenced by the type of additives employed, the w/b ratio, the mixture's workability, and the fabrication procedure, as previously mentioned. The choice of binders directly impacts the workability of pastes [60]. In the context of this study, where the specimens were not subjected to vibration during fabrication, the incorporation of alternative binders led to an increase in entrapped air within the mixes. Consequently, this phenomenon contributed to the observed higher porosity levels in the samples. This may suggest that the mixing procedure should not be uniform for every binder type.

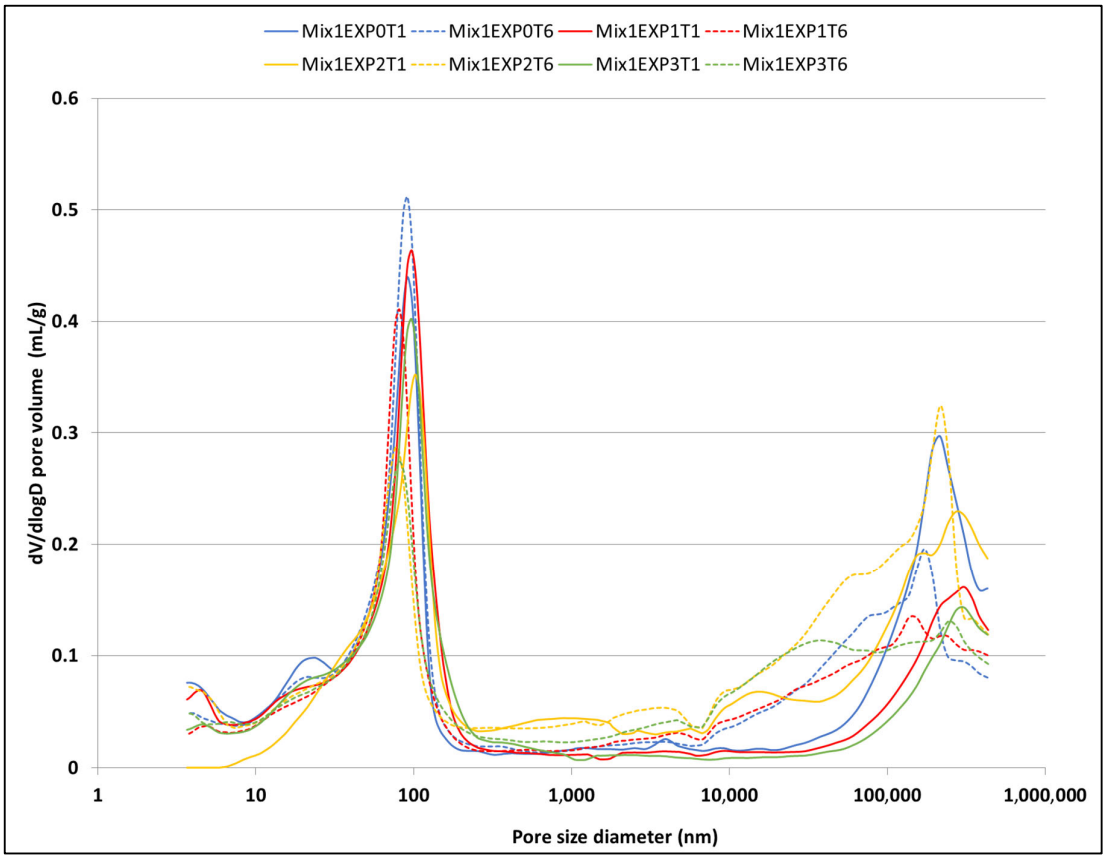

Figure 9. The porosity distribution of the reference mix (Mix1) at both day 1 and day 25 under different exposure conditions.

A 25-day immersion in water (EXP0) increased the overall porosity due to the ongoing hydration process and the creation of hydrated compounds. A noticeable decline in pores with dimensions smaller than 10 µm was obvious across all four mixes.

When considering the impacts of both chloride and sulfate attacks, alterations in total porosity and its distribution are heavily contingent upon various factors, such as CH dissolution, C-S-H decalcification, AFm consumption, ettringite and gypsum formation rates, the emergence of cracks [46], and the ongoing hydration process, particularly considering the early age of the samples.

Figure 8 reveals that when chloride and sulfate were present (EXP1, EXP2, and EXP3), the total porosity of cement aggregates, constituting the exposed powders, decreased after one day of exposure when compared to the ones exposed to water. This decrease was related to the formation of ettringite, gypsum, and Friedel's salt [29]. However, after 25 days of exposure, an increase in total porosity was observed in the four mixes. This was attributed to the excessive formation of expansive products that led to expansion and cracking, as well as the dissolution of CH, decalcification of C-S-H, and consumption of AFm that led to an increase in porosity, although hydration was still in process [12,18,61]. These results are in accordance with the chemical investigations explained in previous sections. In this case, an examination of pore size distribution reveals a reduction in both micropores and small pores to medium capillary pores.

This phenomenon can be attributed to the formation of expansive products within these pore categories. These findings align with the conclusions drawn from the earlier referenced studies in this section [12,18,29,61], and with results obtained from the other analytical techniques used in this study.

Returning to the influence of sulfate and chloride, it is apparent that the reduction in porosity is more significant when both sulfate and chloride are present simultaneously. This

is compared to when only sulfate is present, especially after 1 day of exposure. Nonetheless, upon closer examination of the difference between T1 and T6 within each exposure condition (EXP2 and EXP3) individually, the increase in porosity was more pronounced in specimens solely exposed to sulfate. Moreover, when comparing exposure conditions with sulfate presence at day 25, it was noted that EXP2 exhibited higher porosity than EXP3. This difference in porosity was particularly pronounced in Mix1, revealing the highest porosity difference between the two exposure conditions at day 25, as depicted in Figure 8a. Following this, Mix2 exhibited a difference of 0.8% (Figure 8b), Mix3 showed a difference of 0.3% (Figure 8c), and Mix4 displayed a difference of 0.2% (Figure 8d). This observation implies that the detrimental effects, notably, crack formations and the increase in porosity, are more substantial when sulfate is present alone, although in EXP 3 chloride was present and therefore also generated an increase in porosity in addition to the effect of the sulfate. This suggests that the combination of chloride and sulfate mitigates sulfate-induced damage, resulting in fewer cracks than when only sulfate is present, and might also confirm the inhibition of chloride binding in EXP3, as revealed in Section 3.4.

4. Discussion

The pH elevation in the solutions provides strong evidence of ongoing chemical reactions. Furthermore, this phenomenon was verified by the observed visual color changes (shown in Figure 3).

The TGA test results strongly indicated a substantial consumption of portlandite in the presence of sulfate ions. Concurrently, under identical exposure conditions, AFm was completely depleted. Also, at temperatures below 200 °C on the TGA curve, a significant loss of mass was observed in comparison to EXP0 and EXP1, indicating the formation of ettringite. The FTIR analysis corroborated these findings by revealing significant ettringite formation when subjected solely to sulfate exposure. Interestingly, the corresponding pH levels in this scenario were notably elevated, suggesting heightened kinetics in the chemical reactions between sulfate and cementitious materials. Turning to porosity, a more pronounced increase was observed in specimens exposed solely to sulfate after 25 days. This signifies chloride's mitigating influence on sulfate attack. This observation aligns well with the depletion of sulfate ions in the sulfate-only solution, as monitored through Raman spectroscopy, which can be an easy way to monitor the kinetics of sulfate attack.

The FTIR analysis results revealed the presence of Friedel's salt exclusively in the mixes exposed to chloride. Additionally, a concurrent reduction in portlandite content was identified, which can be linked to the outcomes of the porosity test. In EXP3, the rise in porosity, when compared to EXP2, was relatively modest, despite the presence of chloride along with sulfate, which also causes an increase in the porosity (double effect of sulfate and chloride). This could potentially indicate that, apart from the minimal formation of ettringite, the Friedel's salt formation (binding of chloride ions) was significantly low or possibly absent, as implied by the FTIR findings. The co-presence of sulfate with chloride could expedite the diffusion of chloride ions due to the absence of bound chloride ions.

While no substantial differences were observed among the various mixes regarding chemical reactions, it is worth noting that the inclusion of multiple SCMs postponed ettringite formation. This resulted in better stability in terms of porosity changes (especially in Mix3), and improved the mixes' resistance to attacks.

The comprehensive analysis of the chemical transformations triggered by sulfate and chloride exposure in these low-carbon cementitious powders has provided a foundational understanding of how these ions interact with cement-based materials. However, it is crucial to expand the investigation to encompass larger solid samples, allowing for a more comprehensive exploration of the physicochemical impact of sulfate and chloride within a complex matrix that mimics real-world conditions. A critical area that requires focused attention is the transfer properties governing the diffusion and migration of sulfate and chloride ions within the cement matrix. These transfer properties play a pivotal role in

determining the extent of ion penetration, their interaction with hydration products, and the resulting chemical alterations influencing the material properties themselves.

In order to better understand the chemical changes that occurred, a schematic representation is shown in Figure 10.

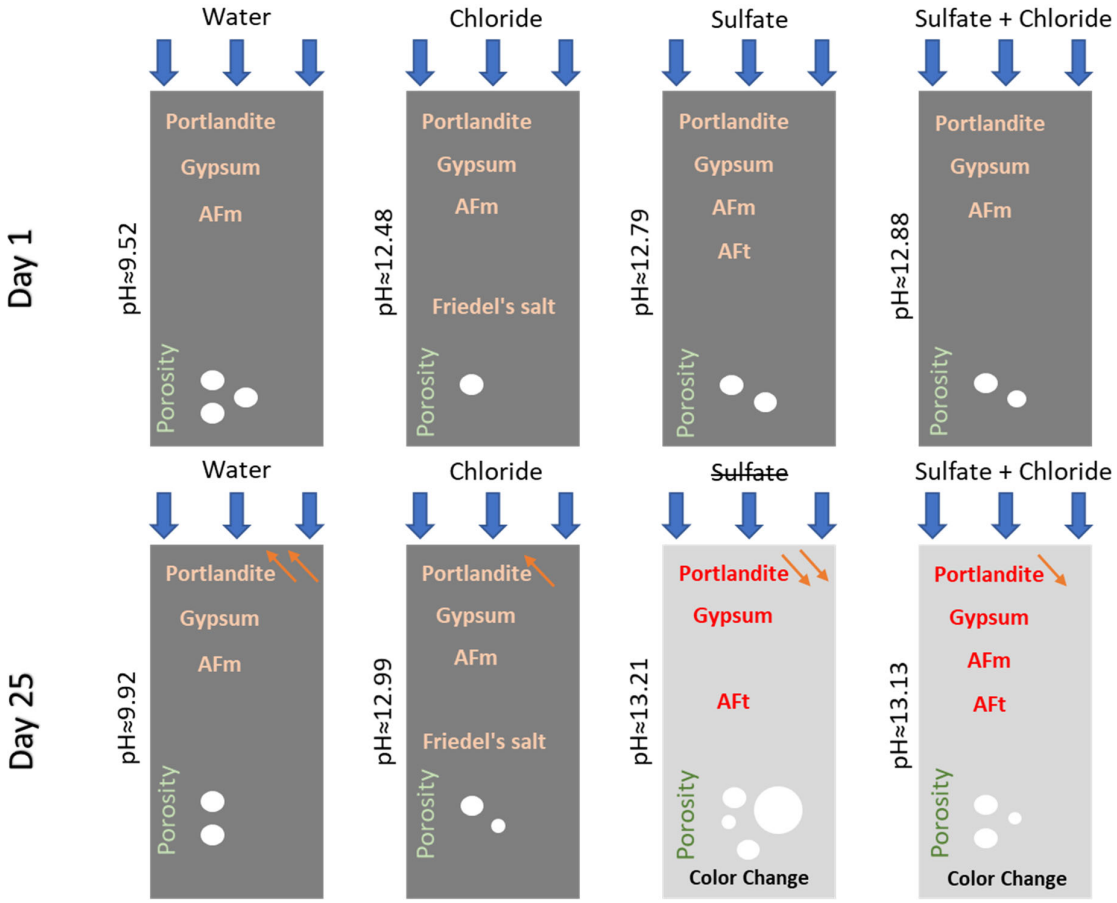

Figure 10. Schematic illustration of the chemical changes that occurred in Mix1 on both day 1 and day 25 in the four different environments.

5. Conclusions

The primary objective of this study was to gain deeper insights into the chemical reactions induced by the combined effect of chloride and sulfate ions on low-carbon cementitious materials. To that end, this study assesses the effectiveness of SCM blends by utilizing pure Portland cement, and binary, ternary, and quaternary pastes. Powders extracted from the pastes at an early age were exposed to various environmental conditions and compared. Based on the findings obtained during this investigation, the following conclusions can be drawn:

- In the sole presence of sulfate, a substantial reduction in portlandite and AFm content was observed, accompanied by a notable formation of ettringite. Furthermore, a marked increase in porosity was observed, and the complete depletion of sulfate ions from the solution was detected (Mix1) by Raman spectroscopy.
- The simultaneous presence of chloride and sulfate ions had a mitigating effect on the sulfate attack on the cementitious materials.
- The FTIR analysis method detected the formation of Friedel's salt and the consumption of portlandite in the presence of chloride ions alone. However, this phenomenon was not observed when sulfate and chloride ions were coupled.
- The presence of sulfate ions accelerates the attack of chloride ions by inhibiting the binding of free chloride ions.

- The incorporation of multiple SCM resulted in a lesser pH increase, a delay in ettringite formation, and a reduction in crack generation. This led to an enhancement of the materials' resistance to attacks.

Future research should include a full study on the combined effects of sulfate and chloride on low-carbon cementitious materials, addressing both chemical reactions and physical processes (physico-chemical properties). It is imperative that not only the chemical interactions are considered, but also the physical aspects, such as the penetration rates of chloride and sulfate ions into the cementitious matrix, because this phenomenon highly impacts the effects of the coupling of sulfate and chloride on cementitious materials. A comprehensive approach will provide a more complete understanding of the complex interplay between these ions and their influence on the properties and durability of concrete.

Author Contributions: Validation, conceptualization, methodology, writing—review and editing, O.O.M., M.M. and M.Q.; writing—original draft preparation, investigation, and formal analysis, F.E.I.; supervision, O.O.M. All authors have read and agreed to the published version of the manuscript.

Funding: This research received no external funding.

Institutional Review Board Statement: Not applicable.

Informed Consent Statement: Not applicable.

Data Availability Statement: Not applicable.

Conflicts of Interest: The authors declare no conflict of interest.

References

1. Tang, S.; Yao, Y.; Andrade, C.; Li, Z. Recent durability studies on concrete structure. *Cem. Concr. Res.* **2015**, *78*, 143–154. [CrossRef]
2. Al-Kheetan, M.J.; Rahman, M.M. Integration of Anhydrous Sodium Acetate (ASAc) into Concrete Pavement for Protection against Harmful Impact of Deicing Salt. *JOM* **2019**, *71*, 4899–4909. [CrossRef]
3. Mehta, P.K.; Monteiro, P.J. *Concrete: Microstructure, Properties, and Materials*; McGraw-Hill Education: New York, NY, USA, 2014.
4. Li, Z.; Zhou, X.; Ma, H.; Hou, D. *Advanced Concrete Technology*; Wiley: Hoboken, NJ, USA, 2022; ISBN 9780470437438.
5. El Inaty, F.; Baz, B.; Aouad, G. Long-term durability assessment of 3D printed concrete. *J. Adhes. Sci. Technol.* **2022**, *37*, 1921–1936. [CrossRef]
6. Sun, W.; Mu, R.; Luo, X.; Miao, C. Effect of chloride salt, freeze–thaw cycling and externally applied load on the performance of the concrete. *Cem. Concr. Res.* **2002**, *32*, 1859–1864. [CrossRef]
7. Sun, W.; Zhang, Y.; Yan, H.; Mu, R. Damage and damage resistance of high strength concrete under the action of load and freeze-thaw cycles. *Cem. Concr. Res.* **1999**, *29*, 1519–1523. [CrossRef]
8. Le Bellégo, C.; Pijaudier-Cabot, G.; Gérard, B.; Dubé, J.-F.; Molez, L. Coupled Mechanical and Chemical Damage in Calcium Leached Cementitious Structures. *J. Eng. Mech.* **2003**, *129*, 333–341. [CrossRef]
9. Metalssi, O.O.; Touhami, R.R.; Barberon, F.; de Lacaillerie, J.-B.D.; Roussel, N.; Divet, L.; Torrenti, J.-M. Understanding the degradation mechanisms of cement-based systems in combined chloride-sulfate attack. *Cem. Concr. Res.* **2023**, *164*, 107065. [CrossRef]
10. Lee, S.-T.; Park, D.-W.; Ann, K.-Y. Mitigating effect of chloride ions on sulfate attack of cement mortars with or without silica fume. *Can. J. Civ. Eng.* **2008**, *35*, 1210–1220. [CrossRef]
11. Ramezanianpour, A.A.; Riahi Dehkordi, E. Effect of Combined Sulfate-Chloride Attack on Concrete Durability-A Review. *AUT J. Civ. Eng.* **2017**, *1*, 103–110. [CrossRef]
12. Jabbour, M.; Metalssi, O.O.; Quiertant, M.; Baroghel-Bouny, V. A Critical Review of Existing Test-Methods for External Sulfate Attack. *Materials* **2022**, *15*, 7554. [CrossRef]
13. Ragoug, R.; Metalssi, O.O.; Barberon, F.; Torrenti, J.-M.; Roussel, N.; Divet, L.; de Lacaillerie, J.-B.D. Durability of cement pastes exposed to external sulfate attack and leaching: Physical and chemical aspects. *Cem. Concr. Res.* **2019**, *116*, 134–145. [CrossRef]
14. Metalssi, O.O.; Ragoug, R.; Barberon, F.; de Lacaillerie, J.-B.D.; Roussel, N.; Divet, L.; Torrenti, J.-M. Effect of an Early-Age Exposure on the Degradation Mechanisms of Cement Paste under External Sulfate Attack. *Materials* **2023**, *16*, 6013. [CrossRef] [PubMed]
15. Neville, A. Chloride attack of reinforced concrete: An overview. *Mater. Struct.* **1995**, *28*, 63–70. [CrossRef]
16. Al-Kheetan, M.J.; Rahman, M.M.; Chamberlain, D.A. Fundamental interaction of hydrophobic materials in concrete with different moisture contents in saline environment. *Constr. Build. Mater.* **2019**, *207*, 122–135. [CrossRef]
17. Lothenbach, B.; Bary, B.; Le Bescop, P.; Schmidt, T.; Leterrier, N. Sulfate ingress in Portland cement. *Cem. Concr. Res.* **2010**, *40*, 1211–1225. [CrossRef]

18. Yu, C.; Sun, W.; Scrivener, K. Mechanism of expansion of mortars immersed in sodium sulfate solutions. *Cem. Concr. Res.* **2013**, *43*, 105–111. [CrossRef]
19. Gu, Y.; Metalssi, O.O.; Martin, R.-P.; Fen-Chong, T.; Dangla, P. Locating ettringite due to DEF at the pore scale of cement paste by heat-based dissolution tests. *Constr. Build. Mater.* **2020**, *258*, 120000. [CrossRef]
20. Cherif, R.; Hamami, A.E.A.; Aït-Mokhtar, A.; Bosschaerts, W. Thermodynamic equilibria-based modelling of reactive chloride transport in blended cementitious materials. *Cem. Concr. Res.* **2022**, *156*, 106770. [CrossRef]
21. Wilson, W.; Gonthier, J.N.; Georget, F.; Scrivener, K.L. Insights on chemical and physical chloride binding in blended cement pastes. *Cem. Concr. Res.* **2022**, *156*, 106747. [CrossRef]
22. Stroh, J.; Meng, B.; Emmerling, F. Deterioration of hardened cement paste under combined sulphate-chloride attack investigated by synchrotron XRD. *Solid State Sci.* **2016**, *56*, 29–44. [CrossRef]
23. Mavropoulou, N.; Katsiotis, N.; Giannakopoulos, J.; Koutsodontis, K.; Papageorgiou, D.; Chaniotakis, E.; Katsioti, M.; Tsakiridis, P. Durability evaluation of cement exposed to combined action of chloride and sulphate ions at elevated temperature: The role of limestone filler. *Constr. Build. Mater.* **2016**, *124*, 558–565. [CrossRef]
24. Dehwah, H.; Maslehuddin, M.; Austin, S. Long-term effect of sulfate ions and associated cation type on chloride-induced reinforcement corrosion in Portland cement concretes. *Cem. Concr. Compos.* **2002**, *24*, 17–25. [CrossRef]
25. Geng, J.; Easterbrook, D.; Li, L.-Y.; Mo, L.-W. The stability of bound chlorides in cement paste with sulfate attack. *Cem. Concr. Res.* **2015**, *68*, 211–222. [CrossRef]
26. De Weerdt, K.; Orsáková, D.; Geiker, M. The impact of sulphate and magnesium on chloride binding in Portland cement paste. *Cem. Concr. Res.* **2014**, *65*, 30–40. [CrossRef]
27. Shaheen, F.; Pradhan, B. Influence of sulfate ion and associated cation type on steel reinforcement corrosion in concrete powder aqueous solution in the presence of chloride ions. *Cem. Concr. Res.* **2017**, *91*, 73–86. [CrossRef]
28. Tumidajski, P.; Chan, G. Effect of sulfate and carbon dioxide on chloride diffusivity. *Cem. Concr. Res.* **1996**, *26*, 551–556. [CrossRef]
29. Ran, B.; Omikrine-Metalssi, O.; Fen-Chong, T.; Dangla, P.; Li, K. Pore crystallization and expansion of cement pastes in sulfate solutions with and without chlorides. *Cem. Concr. Res.* **2023**, *166*, 107099. [CrossRef]
30. Al-Amoudi, O.S.B.; Maslehuddin, M.; Abdul-Al, Y.A. Role of chloride ions on expansion and strength reduction in plain and blended cements in sulfate environments. *Constr. Build. Mater.* **1995**, *9*, 25–33. [CrossRef]
31. Xu, J.; Zhang, C.; Jiang, L.; Tang, L.; Gao, G.; Xu, Y. Releases of bound chlorides from chloride-admixed plain and blended cement pastes subjected to sulfate attacks. *Constr. Build. Mater.* **2013**, *45*, 53–59. [CrossRef]
32. Habert, G.; Miller, S.A.; John, V.M.; Provis, J.L.; Favier, A.; Horvath, A.; Scrivener, K.L. Environmental impacts and decarbonization strategies in the cement and concrete industries. *Nat. Rev. Earth Environ.* **2020**, *1*, 559–573. [CrossRef]
33. Bojana, B.; Julian, M.A.; Jonathan, M.C. Designing Climate Change Mitigation Plans That Add Up. *Environ. Sci. Technol.* **2013**, *47*, 8062–8069. [CrossRef]
34. Marey, H.; Kozma, G.; Szabó, G. Effects of Using Green Concrete Materials on the CO_2 Emissions of the Residential Building Sector in Egypt. *Sustainability* **2022**, *14*, 3592. [CrossRef]
35. Bogue, R.H. The Chemistry of Portland Cement. Second Edition. *Soil Sci.* **1955**, *79*, 322. [CrossRef]
36. *EN 197-1:2011*; Cement—Part 1: Composition, Specifications and Conformity Criteria for Common Cements. European Committee for Standardization: Brussels, Belgium, 2011.
37. NF EN 196-1:2016; Methods of Testing Cement—Part 1: Determination of Strength. Available online: https://www.boutique.afnor.org/en-gb/standard/nf-en-1961/methods-of-testing-cement-part-1-determination-of-strength/fa184622/57803 (accessed on 27 September 2023).
38. Mehta, P.K. Evaluation of Sulfate-Resisting Cements by a New Test Method. *J. Proc.* **1975**, *72*, 573–575.
39. Brown, P.W. An evaluation of the sulfate resistance of cements in a controlled environment. *Cem. Concr. Res.* **1981**, *11*, 719–727. [CrossRef]
40. Delagrave, A.; Pigeon, M.; Marchand, J.; Revertégat, É. Influence of chloride ions and pH level on the durability of high performance cement pastes (Part II). *Cem. Concr. Res.* **1996**, *26*, 749–760. [CrossRef]
41. Behnood, A.; Van Tittelboom, K.; De Belie, N. Methods for measuring pH in concrete: A review. *Constr. Build. Mater.* **2016**, *105*, 176–188. [CrossRef]
42. Bhatty, J.; Taylor, P. Sulfate Resistance of Concrete Using Blended Cements or Supplementary Cementitious Materials (PCA R&D Serial No. 2916a). Article PCA R&D Serial No. 2916a. 2006. Available online: https://trid.trb.org/view/795858 (accessed on 23 August 2023).
43. Mehta, P.; Pirtz, D.; Polivka, M. Properties of alite cements. *Cem. Concr. Res.* **1979**, *9*, 439–450. [CrossRef]
44. Raghav, M.; Park, T.; Yang, H.-M.; Lee, S.-Y.; Karthick, S.; Lee, H.-S. Review of the Effects of Supplementary Cementitious Materials and Chemical Additives on the Physical, Mechanical and Durability Properties of Hydraulic Concrete. *Materials* **2021**, *14*, 7270. [CrossRef]
45. Dehwah, H.A.F. Influence of Cement Composition on Concrete Durability in Chloride–Sulfate Environments. Ph.D. Thesis, Loughborough University, Loughborough, UK, 1999. Available online: https://repository.lboro.ac.uk/articles/thesis/Influence_of_cement_composition_on_concrete_durability_in_chloride_sulfate_environments/9454499/1 (accessed on 20 August 2023).

46. Gu, Y. Experimental Pore Scale Analysis and Mechanical Modeling of Cement-Based Materials Submitted to Delayed Ettringite Formation and External Sulfate Attacks. Ph.D. Thesis, Université Paris-Est, Champs-sur-Marne, France, 2018. Available online: https://theses.hal.science/tel-02384366 (accessed on 28 July 2023).
47. Gao, Y.; Cui, X.; Lu, N.; Hou, S.; He, Z.; Liang, C. Effect of recycled powders on the mechanical properties and durability of fully recycled fiber-reinforced mortar. *J. Build. Eng.* **2022**, *45*, 103574. [CrossRef]
48. Nochaiya, T.; Sekine, Y.; Choopun, S.; Chaipanich, A. Microstructure, characterizations, functionality and compressive strength of cement-based materials using zinc oxide nanoparticles as an additive. *J. Alloys Compd.* **2015**, *630*, 1–10. [CrossRef]
49. Skaropoulou, A.; Sotiriadis, K.; Kakali, G.; Tsivilis, S. Use of mineral admixtures to improve the resistance of limestone cement concrete against thaumasite form of sulfate attack. *Cem. Concr. Compos.* **2013**, *37*, 267–275. [CrossRef]
50. Santhanam, M.; Cohen, M.D.; Olek, J. Mechanism of sulfate attack: A fresh look: Part 1: Summary of experimental results. *Cem. Concr. Res.* **2002**, *32*, 915–921. [CrossRef]
51. Lothenbach, B.; Scrivener, K.; Hooton, R. Supplementary cementitious materials. *Cem. Concr. Res.* **2011**, *41*, 1244–1256. [CrossRef]
52. Matschei, T.; Lothenbach, B.; Glasser, F. The AFm phase in Portland cement. *Cem. Concr. Res.* **2007**, *37*, 118–130. [CrossRef]
53. Jabbour, M. Multi-Scales Study for the External Sulfatic Attack in Reinforced Concrete Structures. Ph.D. Thesis, Université Paris-Est, Champs-sur-Marne, France, 2019. Available online: https://tel.archives-ouvertes.fr/tel-02956401 (accessed on 21 July 2023).
54. Tang, C.; Ling, T.-C.; Mo, K.H. Raman spectroscopy as a tool to understand the mechanism of concrete durability—A review. *Constr. Build. Mater.* **2021**, *268*, 121079. [CrossRef]
55. Water Molecule Vibrations with Raman Spectroscopy. (n.d.). PhysicsOpenLab. Available online: https://physicsopenlab.org/2022/01/08/water-molecule-vibrations-with-raman-spectroscopy/ (accessed on 19 October 2023).
56. Farcas, F.; Touzé, P. La spectrométrie infrarouge à transformée de Fourier (IRTF). Une méthode intéressante pour la caractérisation des ciments (in French). *Bull. Lab. Ponts Chaussées* **2001**, *230*, 77–88. Available online: http://www.ifsttar.fr/collections/BLPCpdfs/blpc_230_77-88.pdf (accessed on 27 September 2023).
57. Liu, P.; Chen, Y.; Wang, W.; Yu, Z. Effect of physical and chemical sulfate attack on performance degradation of concrete under different conditions. *Chem. Phys. Lett.* **2020**, *745*, 137254. [CrossRef]
58. Yue, Y.; Wang, J.J.; Basheer, P.M.; Bai, Y. Raman spectroscopic investigation of Friedel's salt. *Cem. Concr. Compos.* **2018**, *86*, 306–314. [CrossRef]
59. Gong, F.; Zhang, D.; Sicat, E.; Ueda, T. Empirical Estimation of Pore Size Distribution in Cement, Mortar, and Concrete. *J. Mater. Civ. Eng.* **2013**, *26*, 04014023. [CrossRef]
60. Mark, O.G.; Ede, A.N.; Olofinnade, O.; Bamigboye, G.; Okeke, C.; Oyebisi, S.O.; Arum, C. Influence of Some Selected Supplementary Cementitious Materials on Workability and Compressive Strength of Concrete—A Review. *IOP Conf. Ser. Mater. Sci. Eng.* **2019**, *640*, 012071. [CrossRef]
61. Gollop, R.; Taylor, H. Microstructural and microanalytical studies of sulfate attack. I. Ordinary portland cement paste. *Cem. Concr. Res.* **1992**, *22*, 1027–1038. [CrossRef]